Clinical Neurophysiology 123 (2012) 1745–1754

Contents lists available at SciVerse ScienceDirect

Clinical Neurophysiology

journal homepage: www.elsevier.com/locate/clinph

Electrode and brain modeling in stereo-EEG

Nicolás von Ellenrieder [a,b,*], Leandro Beltrachini [a,b], Carlos H. Muravchik [a,c]

[a] Facultad de Ingeniería, Universidad Nacional de La Plata (UNLP), Argentina
[b] Consejo Nacional de Investigaciones Científicas y Técnicas (CONICET), Argentina
[c] Comisión de Investigaciones Científicas de la Provincia de Buenos Aires (CICpBA), Argentina

ARTICLE INFO

Article history:
Accepted 10 January 2012
Available online 23 February 2012

Keywords:
Stereo-EEG
Depth electrode
Forward problem
Inverse problem
Brain anisotropy

HIGHLIGHTS

- Numerical simulations of stereo-EEG measurements with detailed electrode and brain models were carried out taking into account the physic laws governing the phenomena.
- The perturbation in the electric potential distribution due to the presence of the depth electrode is negligible.
- The heterogeneity and anisotropy of the brain's tissues have a significant effect on the stereo-EEG measurements.

ABSTRACT

Objective: To quantify the perturbation due to the presence of a measuring depth electrode on the intracranial electric potential distribution, and to study the effect of the heterogeneity and anisotropy of the brain tissues' electric conductivity.
Methods: The governing differential equations are solved with the Boundary Elements Method to compute the perturbation on the electric potential distribution caused by the presence of the measuring electrode, and with the Finite Elements Method to simulate measurements in an heterogeneous anisotropic brain model.
Results: The perturbation on the measured electric potential is negligible if the source of electric activity is located more than approximately 1 mm away from the electrode. The error induced by this perturbation in the estimation of the source position is below 1 mm in all tested situations. The results hold for different sizes of the electrode's contacts. The effect of the brain's heterogeneity and anisotropy is more important. In a particular example simulated dipolar sources in the gray matter show localization differences of up to 5 mm between homogeneous isotropic and heterogeneous anisotropic brain models.
Conclusions: It is not necessary to include detailed electrode models in order to solve the stereo-EEG (sEEG) forward and inverse problems. The heterogeneity and anisotropy of the brain electric conductivity should be modeled if possible. The effect of using an homogeneous isotropic brain model approximation should be studied in a case by case basis, since it depends on the electrode positions, the subject's electric conductivity map, and the source configuration.
Significance: This simulation study is helpful for interpreting the sEEG measurements, and for choosing appropriate electrode and brain models; a necessary first step in any attempt to solve the sEEG inverse problem.

1. Introduction

Intracranial electroencephalography (iEEG) is an invasive technique which records the electric activity of the neurons in the brain. It has been used since the first half of the last century in diagnosis and treatment of epilepsy and Parkinson Disease (Engel et al., 2005). Given the far better signal to noise ratio and spatial resolution compared to scalp EEG recordings outside the low-conductivity skull, studies on almost every aspect of brain function are carried out with implanted patients (e.g. Halgren et al., 1994; Bechtereva and Abdullaev, 2000; Lachaux et al., 2003; Engel et al., 2005; Shenoy et al., 2008; Blount et al., 2008; Jerbi et al., 2009). The two main types of clinical iEEG using macroscopic electrodes are electrocorticography (ECoG) and stereotaxic-electroencephalography (sEEG) (Benbadis et al., 2005). In the first case electrodes are placed on the

* Corresponding author. Address: Calle 1 y 47, LEICI, Depto. de Electrotecnia, Facultad de Ingeniería, UNLP, La Plata B1900TAG, Argentina. Tel.: +54 221 4259306; fax: +54 221 4236678.
E-mail address: nellen@ieee.org (N. von Ellenrieder).

1388-2457/$36.00
doi:10.1016/j.clinph.2012.01.019

surface of the cortex, while in sEEG depth needle-like electrodes with multiple contacts are inserted in the brain.

There exists a large knowledge regarding the technique, gained from direct analysis of the recorded signals in humans and animals (e.g. Mitzdorf, 1987; Juergens et al., 1999; Logothetis, 2003; Châtillon et al., 2011), and this knowledge is of great importance for the visual analysis and interpretation of the iEEG recordings performed by expert neurologists. However, there is an increasing interest in solving source estimation problems with iEEG, i.e. solving the iEEG inverse problem, for ECoG recordings (Acar et al., 2008; Zhang et al., 2008; Dümpelmann et al., 2009; Cho et al., 2011) and sEEG recordings (Chang et al., 2005; Litvak et al., 2010). Automatic algorithms to solve the inverse problem need the forward problem solution, i.e. the ability to simulate the measurements that would result from known sources. This requires the numerical solution of the physic laws governing the phenomena. It is important then to select proper models for the measuring electrodes, and to quantify the effect of the measuring electrodes on the electric potential distribution under study. To our knowledge there exist only very crude analysis of these phenomena in the literature for iEEG measurements (Chang et al., 2005; Zaveri et al., 2009).

Scalp electrode properties have been widely studied, both for EEG (Ollikainen et al., 2000; Wendel et al., 2007) and for electrical impedance tomography (Cheng et al., 1989; Somersalo et al., 1992; Paulson et al., 1992). These studies show that the perturbation of the electric potential distribution on the scalp due to the presence of the electrodes is negligible. Then, a good approximation of the forward problem is an ideal point size approximation for the electrodes, which does not modify the electric potential distribution. The reason behind the validity of this approximation is the spatial smoothing effect of the low conductivity skull on the electric potential distribution. The extension of this approximation to intracranial electrodes is not immediate given the much more abrupt spatial distribution of the electric potential inside the skull.

Given that sEEG deep electrodes are typically in contact with different brain tissues (e.g. cortical gray matter, cortical white matter, subcortical nuclei), a detailed model of the brain should take into account the heterogeneity and anisotropy of the electric conductivity of the tissues. The conductivity of the cerebrospinal fluid (CSF) is several times larger than the gray and white matter conductivity, and the fibers tracts in the white matter exhibit a high anisotropy. It is possible to build a brain model that incorporates a detailed electric conductivity map, using Diffusion Tensor Magnetic Resonance Images (DT-MRI) (Tuch et al., 2001). In scalp EEG measurements the heterogeneity and anisotropy of the brain tissue has noticeable effects in the forward problem, the dominant factor being the higher conductivity of the CSF compared to other brain tissues (Wolters et al., 2006). It is reasonable to assume that the effects of the heterogeneity and anisotropy are not smaller in iEEG (Lachaux et al., 2003).

In this work, we investigate the sensitivity of depth electrodes with different contact sizes and for different values of the contact impedance. We also analyze the validity of approximate electrode models. Finally, we present results regarding the effect of heterogeneity and anisotropy of the electric conductivity of the tissues in which the electrodes are inserted, in order to guide the selection of an appropriate brain model.

2. Methods

We study two aspects of the sEEG recordings. First, we study the required detail level of the electrode model in an infinite isotropic medium. Then, we explore how an heterogeneous anisotropic medium affects the measurements. Each situation requires different methods, described in this section.

2.1. Electrode model

We simulate measurements of a depth electrode in an infinite, homogeneous, and isotropic medium. The depth electrode consists in a very thin cylindrical stem with non-conducting walls, interleaved with several conducting contacts. The electrode is inserted into the brain, and the electric potential is recorded at the contacts. The electrode is surrounded by ionic medium, such as intracellular fluids in gray and white matter or cerebrospinal fluid. The equations governing this situation, in an infinite homogeneous medium are (Cheng et al., 1989; Ollikainen et al., 2000)

$$\begin{cases} \sigma\nabla^2\phi(\boldsymbol{x}) = \nabla\cdot\boldsymbol{J}_0(\boldsymbol{x}) & \\ \nabla\phi(\boldsymbol{x})\cdot\boldsymbol{n}(\boldsymbol{x}) = 0 & \boldsymbol{x}\in S_0, \\ \phi(\boldsymbol{x}) + z\sigma\nabla\phi(\boldsymbol{x})\cdot\boldsymbol{n}(\boldsymbol{x}) = \Phi_k & \boldsymbol{x}\in S_k, k=1,\dots,K, \\ \int_{S_k}\nabla\phi(\boldsymbol{y})\cdot\boldsymbol{n}(\boldsymbol{y})ds(\boldsymbol{y}) = 0 & k=1,\dots,K, \end{cases} \tag{1}$$

where σ is the electric conductivity, $\phi(\boldsymbol{x})$ is the electric potential, $\boldsymbol{J}_0(\boldsymbol{x})$ is the primary current, source of the electric activity, $\boldsymbol{n}(\boldsymbol{x})$ is a unitary vector normal to a surface at point $\boldsymbol{x}$, S_0 is the surface of the non-conducting electrode wall, z is the contact impedance between the conducting electrode's contacts and the (ionic) medium, $S_{k,\ k=1,\dots,K}$ are the surfaces of the K electrode's contacts, and Φ_k is the electric potential measured at the k-th contact. The first equation is the Poison differential equation, the second and third equations are the boundary conditions for the non-conducting and conducting surfaces respectively, and the fourth equation imposes a net current of zero through every contact, compatible with a high input impedance of the measuring amplifier.

In the contact surface between media with ionic and electronic conduction a thin, highly resistive layer is formed. The value of the resulting contact impedance is related to the fluid's ionic conductivity. For saline solution the product between the contact impedance and the electric conductivity is nearly constant $z\sigma = 2.4\times10^{-3}$ m (Cheng et al., 1989; Somersalo et al., 1992). We adopted this value for our simulations, with $\sigma = 0.3$ S/m, and $z = 8\times10^{-3}\ \Omega\,\mathrm{m}^2$.

In our simulations we chose a dipolar source model, i.e. $\boldsymbol{J}_0(\boldsymbol{x}) = \boldsymbol{q}\delta(\boldsymbol{x}-\boldsymbol{p})$, where $\boldsymbol{q}$ is the dipole moment (intensity and orientation), $\delta(\cdot)$ is a Dirac delta in 3-D space, and $\boldsymbol{p}$ is the dipole position. While for scalp EEG recordings a dipolar model is appropriate in some occasions (de Munck et al., 1988; Merlet and Gotman, 1999; Kobayashi et al., 2005), we do not believe this is the general case for intracranial recordings. In the latter, the source extent could easily be of the same order as the distance between the source and the electrode, and a dipolar model is expected to perform poorly in this situation. However, distributed sources can be modeled by correctly selected dipole sets (Jerbi et al., 2004; von Ellenrieder et al., 2009). Then, we chose the dipolar source model because the associated results are easy to interpret and to extrapolate to distributed source models.

The differential problem (1) is an exterior problem that cannot be solved with numerical methods that discretize the whole domain, such as finite element or finite difference methods. Instead, we use the Boundary Elements Method (BEM), which is appropriate for solving exterior boundary value problems (Brebbia and Dominguez, 1992). This method requires the differential formulation (1) to be stated as an integral problem (see Appendix A):

$$\begin{aligned} c(\boldsymbol{x})\phi(\boldsymbol{x}) =& 4\pi\phi_0(\boldsymbol{x}) - \int_S \phi(\boldsymbol{y})\nabla\left(\frac{1}{|\boldsymbol{x}-\boldsymbol{y}|}\right)\cdot\boldsymbol{n}(\boldsymbol{y})ds(\boldsymbol{y}) \\ & - \frac{1}{z\sigma}\sum_{k=1}^{K}\int_{S_k}\frac{\phi(\boldsymbol{y})-\Phi_k}{|\boldsymbol{x}-\boldsymbol{y}|}ds(\boldsymbol{y}), \end{aligned} \tag{2}$$

where $S = \bigcup_{k=0}^{K} S_k$ is the surface of the electrode (conducting and non-conducting), $c(\boldsymbol{x})$ takes a value of 4π for points not in the

surface, 2π for points on S, except at the electrode edges where $c(\boldsymbol{x}) = 3\pi/4$. The function $\phi_0(\boldsymbol{x})$ is the electric potential distribution that would be generated by the source in an infinite medium with no electrode present, i.e. for a dipolar source

$$\phi_0(\boldsymbol{x}) = \frac{1}{4\pi\sigma}\frac{\boldsymbol{q}\cdot(\boldsymbol{x}-\boldsymbol{p})}{|\boldsymbol{x}-\boldsymbol{p}|^3}. \quad (3)$$

The unknowns are the K measured potentials, given by

$$\Phi_k = \frac{1}{A_k}\int_{S_k}\phi(\boldsymbol{y})ds(\boldsymbol{y}), \quad k = 1,\ldots,K, \quad (4)$$

where A_k is the surface area of the k-th contact.

We simulated measurements for a typical electrode of cylindrical shape, with 0.5 mm radius and 25 mm length. The electrode had 5 contacts uniformly spaced along the cylinder, the distance between the center of two neighboring contacts was fixed at 5 mm, but the length of the contacts was variable (0.5, 1, 2, or 3 mm). The electric conductivity of the non-conducting walls of the electrode stem was considered null, and infinite for the conducting contacts. To apply the BEM the surfaces were tessellated in 10,984 triangular elements and 5494 nodes (vertices), with local refinement of the mesh in the interface between conducting and non-conducting surfaces. More details regarding the BEM discretization are given in Appendix A.

One of the main objectives of this work is to determine under what conditions a detailed electrode model can be omitted. We define then the unperturbed approximation as the measurements of an hypothetical ideal electrode, with point-size electrode's contacts. The electric potential measured by this ideal electrode approximation (IEA) is given by

$$\Phi_k = \phi_0(\boldsymbol{x}_k), \quad (5)$$

where $\boldsymbol{x}_k$ is the center of the k-th contact. We compare the IEA with the results obtained with the detailed electrode model (DEM) of (4), for different contact impedance values and sizes of the electrode's contacts.

To compare the different simulation scenarios, we computed the sensitivity of the measurements to the source intensity of a dipolar source as a function of the source position $\boldsymbol{p}$,

$$Se(\boldsymbol{p}) = \left|\frac{\partial\Phi_k}{\partial q}\right|, \quad (6)$$

where $q = |\boldsymbol{q}|$ is the intensity of the dipolar source. In this way we build sensitivity maps for the different electrodes. We normalized the sensitivity by its maximum value among all the tested sources, i.e. among the different values of the source parameters $\boldsymbol{q}$ and $\boldsymbol{p}$. The sensitivity computed in this way is a ratio indicating the proportion of the electric potential at a contact to the maximum electric potential at that contact due to a source of the same intensity but at a different position.

Since the final goal is to solve the inverse problem with iEEG data, we also evaluated the effect of the different electrode models in the inverse problem solution. We solved the inverse problem in a very simplified setting, assuming there was no noise and a single dipolar source. The forward problem was solved with the DEM, and the inverse problem was solved adopting the IEA. The solution to the inverse problem was chosen as the point at which the simulated measurements vector (the electric potential in the five electrode's contacts) of the IEA is closest, in l_2-norm, to the simulated measurements vector of the DEM.

2.2. Brain model

For the selection of the brain model, our main interest is to compare a detailed model including the heterogeneity and anisotropy of the electric conductivity of the tissues with an homogeneous and isotropic model. Since the first model is more realistic, we adopted it as the reference. The homogeneous isotropic model is considered an approximation.

When a detailed model of the brain is adopted, including the electric conductivity heterogeneity and anisotropy of the tissues, the governing differential equation for a dipolar source is given by

$$\nabla\cdot(\bar{\sigma}(\boldsymbol{x})\nabla\phi(\boldsymbol{x})) = \nabla\cdot(\boldsymbol{q}\delta(\boldsymbol{x}-\boldsymbol{p})), \quad (7)$$

where $\bar{\sigma}(\boldsymbol{x})$ is the electric conductivity tensor at point $\boldsymbol{x}$. Since the BEM is not appropriate to handle heterogeneity in the domain, to solve this differential problem we resort to the Finite Elements Method (FEM) (Wolters et al., 2006). The same formulation holds for the homogeneous isotropic brain model, simply considering the conductivity tensor $\bar{\sigma}(\boldsymbol{x}) = \sigma I_3$, where I_3 is a 3×3 identity matrix, and $\boldsymbol{x}$ is any point in the brain.

As the electrode model we adopted the IEA defined in (5). Hence, the geometric model did not include the electrode. We used an average head model built from a sample of 152 MRIs of typical participants provided by the International Consortium of Brain Mapping (ICBM) (Mazziotta et al., 2001). The scalp and skull surfaces were extracted from the image using the brain extraction tool (Jenkinson et al., 2005) and then corrected using MeshLab.

We built an homogeneous isotropic brain model (HoIBM) and an heterogenous anisotropic brain model (HeABM). The HoIBM assumes the electric conductivity of the brain is 0.33 S/m (Dannhauer et al., 2011). The HeABM incorporates the heterogeneity and anisotropy using a diffusion tensor atlas based on 81 healthy participants (Mori et al., 2008) co-registered with the ICBM model. We considered the electrical conductivity as a tensor field through a linear transformation of the diffusion tensor eigenvalues (Tuch et al., 2001).

For both models, the scalp and skull were modeled as isotropic homogeneous layers of electric conductivity of 0.33 and 0.0096 S/m respectively (Dannhauer et al., 2011). The models were tessellated using the ISO2Mesh toolbox (Fang and Boas, 2009), resulting in a tetrahedral mesh with 2 mm mean side length, with a local refinement in the neighborhood of the electrode limiting the side length to 1 mm. This resulted in models with 774,020 tetrahedral elements and 125,624 nodes. For the HeABM the conductivity tensor was considered constant in each element.

To illustrate the heterogeneity and anisotropy of the HeABM we compute the mean conductivity $MC(\boldsymbol{x}) = \mathrm{tr}\{\bar{\sigma}(\boldsymbol{x})\}/3$ and the anisotropy factor $FA(\boldsymbol{x}) = \sqrt{\frac{(\lambda_1-\lambda_2)^2+(\lambda_1-\lambda_3)^2+(\lambda_2-\lambda_3)^2}{2(\lambda_1^2+\lambda_2^2+\lambda_3^2)}}$ respectively, where λ_1, λ_2, and λ_3 are the eigenvalues of the electric conductivity tensor $\bar{\sigma}(\boldsymbol{x})$.

To determine the influence of the heterogeneity and anisotropy of the model we compared the forward and inverse problem solution of both models. We computed the combined sensitivity of all the sensors to the intensity of a dipolar source

$$Se(\boldsymbol{p}) = \sum_{k=1}^{K}\left(\frac{\partial\Phi_k}{\partial q}\right)^2. \quad (8)$$

Note that this measure is proportional to the Fisher Information on the source intensity q when the measurements are corrupted with normal additive noise uncorrelated between electrodes (Kay, 1993).

We also compare the electric potential profile across the electrodes, between models, with the normalized relative difference measure (Meijs et al., 1989)

$$NRDM = \left\|\frac{\Phi_{HoIBM}}{\|\Phi_{HoIBM}\|} - \frac{\Phi_{HeABM}}{\|\Phi_{HeABM}\|}\right\|, \quad (9)$$

where the $\|\cdot\|$ is the l_2 norm, and Φ_{HoIBM} and Φ_{HeABM} are the vectors with the electric potential at the contacts computed as the forward problem solution of both models. For a dipolar source the *NRDM* depends on the source position and orientation, but not on its intensity. The NRDM varies between 0 and 2, it is null when both vectors are equal, 2 when they are collineal but with different sign, and 1 when the vectors are orthogonal.

3. Results

3.1. Electrode model

The described methodology allows us to compute the electric potential distribution generated by any known source, and study how it is perturbed by the presence of the electrode. The example in Fig. 1 shows the current density lines produced by an hypothetical dipolar source near a conducting electrode's contact. The figure was drawn using the line integral convolution technique (Cabral and Leedom, 1993). The intensity of the current density is not evident in this figure, but it quickly decreases with the distance to the source. It can be seen that the direction of the current density lines is modified by the conducting contact of the electrode, becoming normal to the surface. The modification of the current density distribution due to the presence of the electrode is very local, restricted to less than half a millimeter around the electrode.

A result of more interest is the value that the electric potential takes at the contacts, for different source positions and orientations. Fig. 2 shows the sensitivity maps of the electrodes of length 1 and 3 mm. Fig. 2a and b correspond to unipolar measurements and Fig. 2c and d to bipolar measurements. The sensitivity maps show a very fast decrease with the distance to the electrodes. The sensitivity in an infinite and homogeneous medium has axial symmetry, and is maximum for sources in front of the electrode's contact and pointing towards it (or in the opposite direction). The sensitivity for sources with this orientation is shown at the right of the electrode in the figures. Sources with orientation parallel to the electrode's stem generate a signal of almost the same amplitude than the normally oriented ones when placed in front of the boundary between the electrode's contact and the non-conducting wall of the stem. The sensitivity for sources with this orientation is shown in the figures to the left of the electrodes. The sensitivity is null for sources with orientation normal to the plane containing the electrode and the source. In the case of bipolar measurements the sensitivity to sources parallel to the stem is higher for sources located between the electrode's contacts, and the sensitivity to sources with orientation normal to the stem is higher for sources located in front of the electrode's contacts.

We also studied the effect of changes in the contact impedance, finding that the results are not very sensitive to it. Fig. 3 shows the relative difference between the sensitivity computed with the nominal impedance $z_n = 8 \times 10^{-3}\,\Omega\,m^2$, and values ranging from $z \to \infty$ and $z_n = 8 \times 10^{-5}\,\Omega\ m^2$. Note that for the electrode of 1 mm length the contact area is of $3.14 \times 10^{-6}\,m^2$, leading to a nominal contact resistance of approximately 2500 Ω. The results shown on Fig. 3a correspond to sources with the highest absolute error, located in front of one electrode and pointing towards it. Fig. 3b shows the spatial distribution of the relative difference between the sensitivity with nominal impedance and the sensitivity for impedance one order of magnitude lower $z = 8 \times 10^{-4}\,\Omega\,m^2$. Difference larger than 1% are limited to the vicinity (less than 2 mm) of the electrode.

We found that the IEA given by (5), is very good for sources located farther than 1 or 2 mm from the electrode, and that the effect of the electrode size is not very important except in the immediacy of the electrode. Fig. 4a shows the sensitivity for sources located in front of the electrode and pointing towards it, for the IEA and for DEM of different contact sizes. The error of the IEA is restricted to the vicinity of the electrode, and seems negligible at 2 mm from it. The error of larger electrodes is a bit larger, but the dependence with size is not direct, and varies for sources at different positions. The logarithmic scale in both axes highlights the quadratic decrease of the sensitivity with the distance to the electrode. Fig. 4b shows the spatial distribution of the IEA relative error for electrodes with 1 mm contacts. Note that the relative error may seem large for sources in front of the contact and with orientation parallel to the electrode, but the absolute value of the error for these source is actually very small since the sensitivity to them is low, as seen in Fig. 2a.

Another point of interest is the effect that the IEA has in the inverse problem. We found that the errors are negligible from a practical point of view, regardless of the contact size. In Fig. 5 we show the localization error of dipolar sources when the IEA is adopted for solving the inverse problem, for electrode contacts of 1 and 3 mm length. The localization error is in the worst case less than half a millimeter, and much smaller for sources 1 or 2 mm away from the electrode. A localization error of half a millimeter for sources located at 1 or 2 mm from the electrode may be large from a mathematical point of view, but it is not significant from a practical one.

3.2. Brain model

We studied the effect of the heterogeneity and anisotropy of the electric conductivity of the brain model. We simulated sEEG measurements for 10 contacts on a depth electrode placed in the right

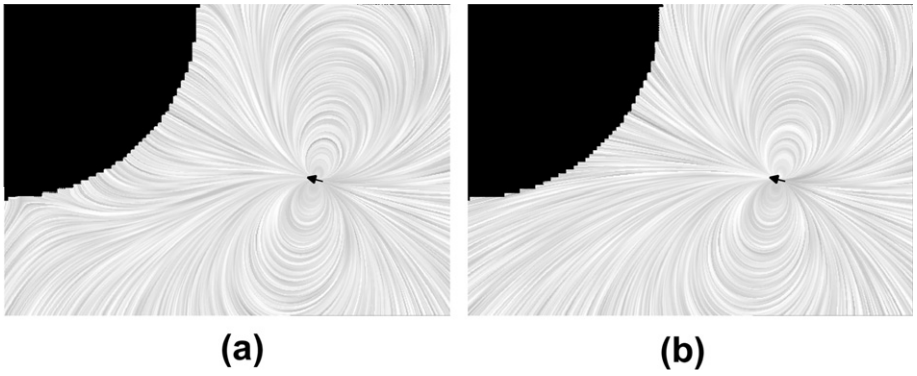

Fig. 1. Current density lines due to a dipolar source near the electrode. The figure shows how the current density distribution is disturbed by the presence of the electrode, but only in its close proximity. The electrode is depicted in black at the upper left corner, it has a 0.5 mm radius. (a) Current density lines when the electrode is present. (b) Current density lines if the electrode were not present. The current intensity is also modified, but it is not evident in the figure.

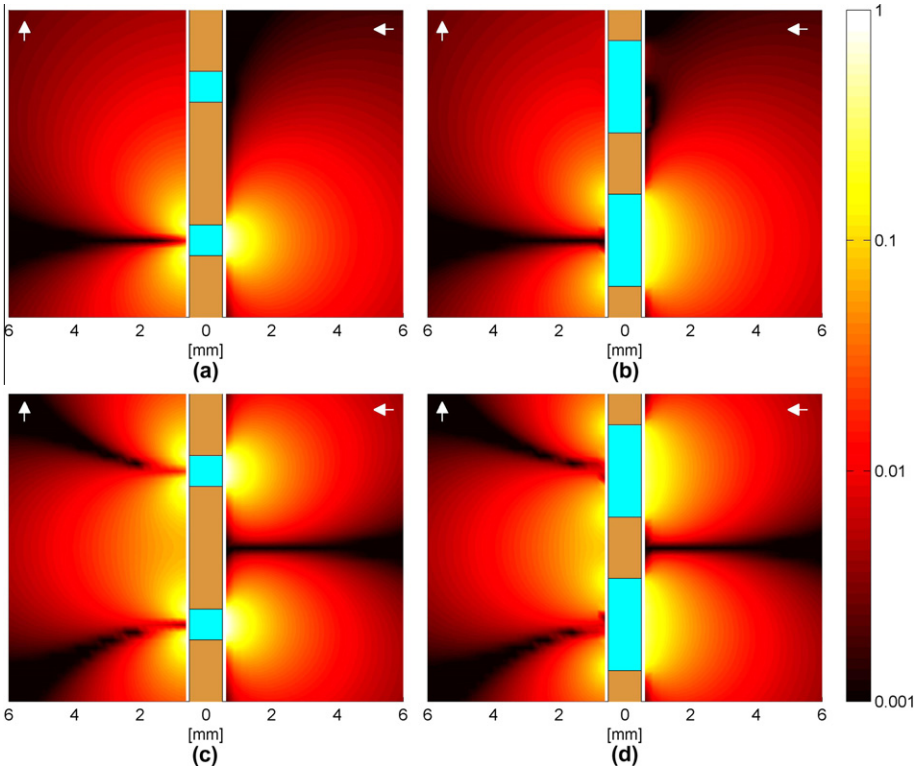

Fig. 2. Sensitivity maps of the depth electrodes. The color (or gray level – in the printed version of this article) of each point indicates the normalized sensitivity of the electrode to a dipolar source located at that point. The results to the left of the electrodes correspond to sources with dipolar moment parallel to the electrode stem, to the right of the electrode results correspond to sources with dipolar moment pointing towards the electrode stem. The arrows on the corners indicate the dipolar moment orientation. The diameter of the electrode is 1 mm, the conducting contacts are depicted in light blue color (or – in the printed version of this article – light gray in the electrode). (a) Unipolar sensitivity, 1 mm contacts. (b) Unipolar sensitivity, 3 mm contacts. (c) Bipolar sensitivity, 1 mm contacts. (d) Bipolar sensitivity, 3 mm contacts.

temporal lobe, as shown in Fig. 6a. The color (or – in the printed version of this article – gray level) scale of the image indicates the mean conductivity of the head model, and the white rectangle, shown in more detail in Fig. 6b corresponds to the analyzed source positions. The dipolar moment of the analyzed sources is oriented parallel to the electrode.

The sensitivity of the electrodes to the source intensity is higher for sources located in regions with lower conductivity. This is reasonable since a primary current density in a region with low conductivity (high resistivity) generates an electric potential of higher amplitude than the same primary current in a high conductivity region. Fig. 7 shows the combined sensitivity (6) of all the contacts for both brain models, the HoIBM in Fig. 7a, and the HeABM in 7b. The sensitivity differences seem to be explained by the mean conductivity of the regions, shown in Fig. 6b.

While the sensitivity to the source intensity is correlated to the mean conductivity, the distribution of the electric potential at the different contacts seems more correlated to the anisotropy of the medium. In Fig. 8a we show the anisotropy factor of the medium, and in Fig. 8b the NRDM of the difference between the HoIBM and

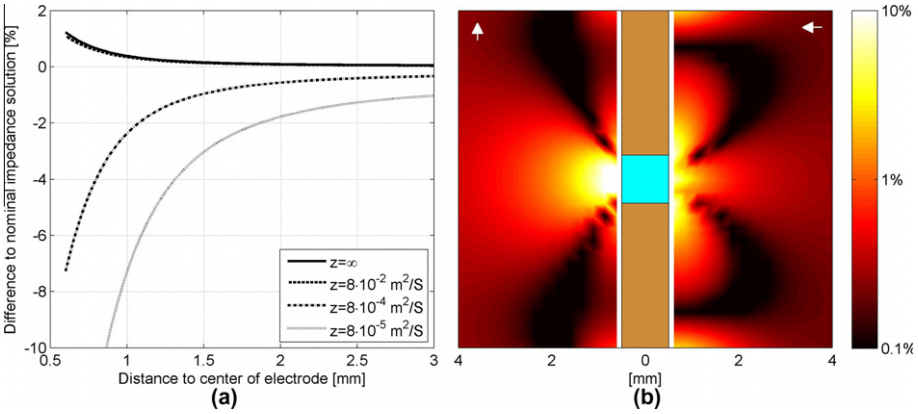

Fig. 3. Effect of contact impedance value. (a) Relative difference between results obtained with the nominal contact impedance $z_n = 8 \times 10^{-3}\ \Omega\,m^2$ compared to results for other contact impedance values. Results correspond to dipolar sources with moment pointing towards the electrode and located in front of the contacts; these source show the highest absolute difference. (b) Relative error maps between the $z = 8 \times 10^{-4}\ \Omega\,m^2$ and the $z_n = 8 \times 10^{-3}\ \Omega\,m^2$ results. To the left of the electrode results for sources with moment parallel to the electrode stem and to the right results for sources with moment pointing towards the electrode stem, as indicated by the arrows on the corners.

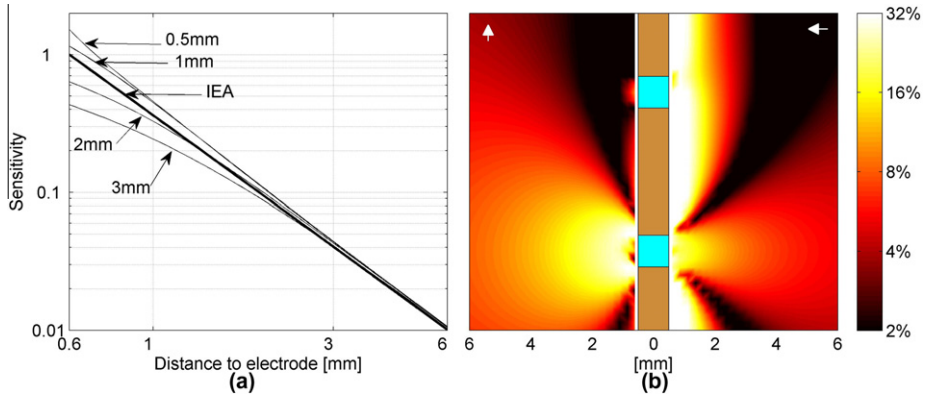

Fig. 4. Effect of electrode size, and quality of ideal electrode approximation (IEA). (a) Sensitivity as a function of the distance to the center of the electrode, for dipolar sources with moment pointing towards the electrode stem located in front of a contact. Results are shown for several contact sizes and for the point approximation. (b) Relative error of the point approximation for electrodes with 1 mm contacts. To the left of the electrode results for sources with moment parallel to the electrode stem and to the right results for sources with moment pointing towards the electrode stem, as indicated by the arrows on the corners.

the HeABM results. The NRDM is very high in regions of high anisotropy, indicating that the anisotropy of the tissue has an important effect on the electric potential distribution.

The errors in the estimation of the source location can be significative if the heterogeneity and anisotropy of the medium is ignored. Fig. 9 shows the localization error when the simulated measurements are computed with the HeABM and the source localization is performed using the HoIBM. The sources are located on the same brain slice than those used in the forward problem analysis, and also have a dipolar moment parallel to the electrodes. Due to the poor azimuthal resolution of the depth electrode around its axis, for the analysis of the inverse problem performance we assume three depth electrodes with ten contacts each are used. These electrodes are placed separated by 30 mm, forming an equilateral triangle. The top electrode is in the same plane as the sources, the other two are outside the plane. The projections of these two electrodes, located 15 mm above and below the plane, are shown at the bottom of Fig. 9a. We see in this figure that the localization error associated to the HoIBM can reach up to 15 mm. However, the largest errors correspond to unlikely source positions, i.e. outside the gray matter. The white lines in the figure represent a crude partition of the brain tissues, gray matter being located on the right and bottom of the slice. In Fig. 9b we analyze the relationship between the localization error and the mean conductivity and anisotropy factor of the position at which the source is located. The largest errors correspond to regions with high mean conductivity, i.e. CSF. White matter regions, with high anisotropy, show a mixture of medium and small errors. The localization error for sources of physiological significance associated to gray matter (low mean conductivity and anisotropy factor), is smaller; a few of these sources have a localization error between 5 and 10 mm, but for most of them it is less than 5 mm.

4. Discussion

The simulation results show that the perturbation induced by the presence of the electrode is quite local. The electric potential distribution of a particular source is modified only in the close neighborhood of the electrode. Also, the measurements of the electrode's contacts depend on the electrode model only if the source of electric activity is located within 1 or 2 mm of the electrode. Note that the difference between unipolar and bipolar configurations shown in Fig. 2, while crucial for a visual interpretation of the depth electrode recordings, is of little consequence if the inverse problem is solved automatically.

One important consequence of the local character of the perturbations due to the presence of the electrode, is that the size (or surface area) of the contacts is not too important from the point of view of the forward or inverse problem. While larger contacts tend to distort the

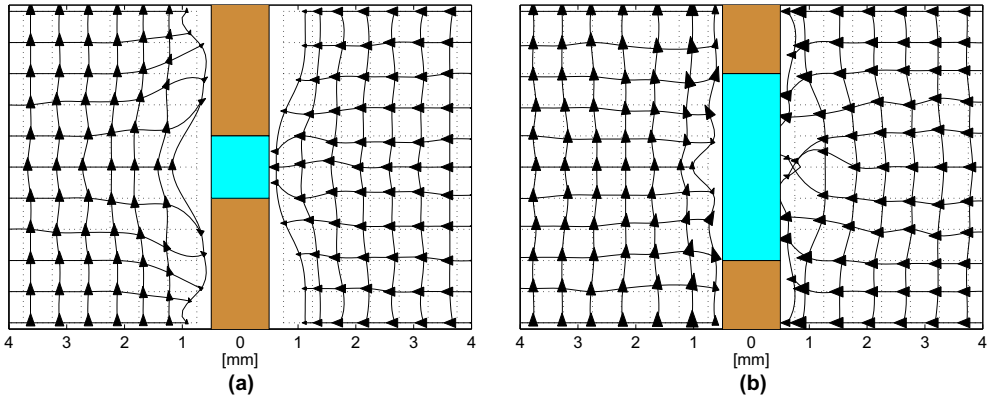

Fig. 5. Effect of point approximation on the inverse problem results. Errors of the inverse problem results for a single dipolar source and no-noise. Measurements simulated with the detailed electrode model and inverse problem solved with the point approximation. The mesh shows the estimated positions for sources on the intersections of the original grid shown in dotted points. The triangles indicate the moment (orientation and intensity) of the estimated dipolar sources. To the left of the electrode results for sources with moment parallel to the electrode stem and to the right results for sources with moment pointing towards the electrode stem. (a) 1 mm contacts and (b) 3 mm contacts.

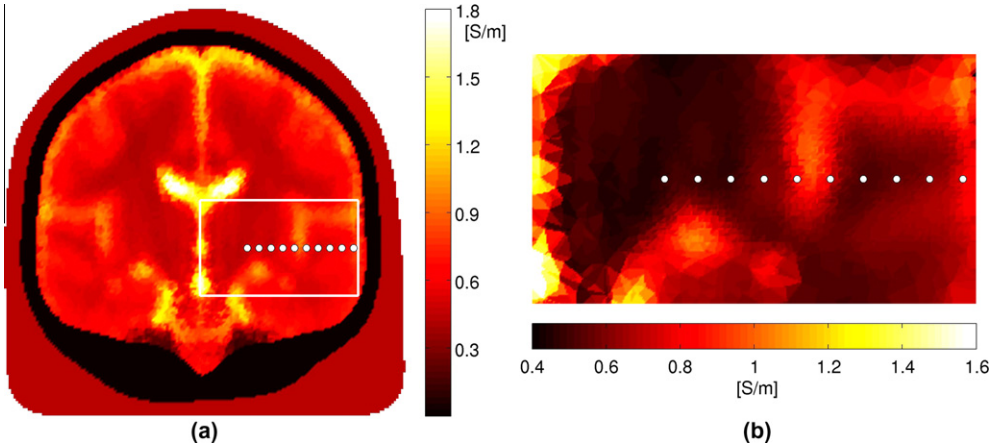

Fig. 6. Mean conductivity value of the head model. (a) Coronal slice showing the MC value of the electric conductivity tensor. The position of ten contacts in the right temporal lobe is shown. (b) Detail of the MC value for the region indicated by a white rectangle on (a).

electric potential a little more, this distortion is still restricted to the proximity of the electrode. This suggests that contacts with large surface area leading to lower impedance on the measuring channels could be used without compromising the quality of inverse problem results. Existing empirical observations in rat sEEG recordings agree with these results (Châtillon et al., 2011).

The contact impedance between ionic and electronic conducting media also has a limited and local effect restricted to the electrode's proximity. The same low sensitivity to the contact impedance value was observed for scalp electrodes (Ollikainen et al., 2000). As seen in Fig. 3, a very good approximation is obtained with an infinite contact impedance, i.e. modeling the conducting electrode's contacts as non-conducting material. This is justified by the high impedance layer formed in the interface between both media, and it explains the low impact of the electrode's contact size discussed in the previous paragraph. If this approximation is used, the whole wall of the electrode stem is non-conducting so the contact size plays no role. It also simplifies the forward problem solution since the last term in (2) vanishes. However, the much simpler ideal electrode approximation discussed in the next paragraph limits the usefulness of this non-conducting contacts approximation.

The main result of this paper is the validation of the IEA given by (5). The simulation results show that an ideal electrode model consisting in sensing the unperturbed electric potential in a point at the center of the electrode's contact is a good approximation to the detailed electrode model. From the forward problem point of view, the IEA is very good for sources located farther than around 1 mm from the electrode surface. And from the inverse problem point of view, the error for sources located less than 1 mm away from the electrode is negligible in practice. Hence, it is not necessary to include the detailed electrode model in the forward problem when the aim is to use the sEEG recordings for source estimation algorithms. This result is important because it allows to avoid the inclusion of the actual electrode in the models. Due to the small electrode radius, the meshes modeling it would need extremely small elements and drastically increase the computational load of any numerical solution of the forward problem.

Adopting the IEA we studied the effect of the electric conductivity heterogeneity and anisotropy of the brain model. We compared forward problem results obtained with an homogeneous isotropic brain model (HoIBM) and with an heterogeneous anisotropic brain model (HeABM). Our results show that the difference between the models could be important. Higher sensitivity is observed for sources located in regions with lower conductivity, and the distribution of the measured electric potentials is highly dependent on the anisotropy of the tissue were the source is located. Regarding these results it is important to note that the region of interest should be restricted to the gray matter, which has low anisotropy and approximately constant conductivity. If we restrict our results to such regions the difference between brain models is much smaller.

From the inverse problem point of view we analyzed the localization error for a single dipolar source, with no noise in the measurements. The localization errors associated to the HoIBM takes values up to 15 mm, but are usually below 5 mm if the sources are restricted to gray matter regions. We must point out that the conductivity tensor maps used in the heterogeneous anisotropic

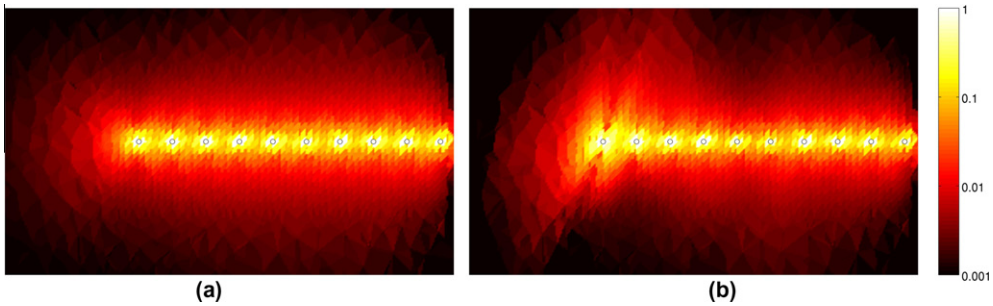

Fig. 7. Joint Sensitivity of the electrode's contacts. The color (or – in the printed version of this article – gray level) of each point indicates the combined sensitivity to a dipolar source at that point. (a) Homogeneous isotropic conductivity brain model. (b) Heterogeneous anisotropic conductivity brain model.

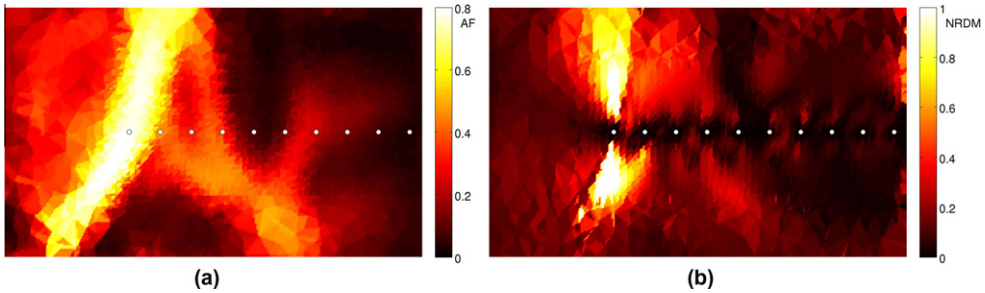

Fig. 8. Electric potential distribution results. (a) Anisotropy factor of the head model. (b) Normalized relative difference measure between isotropic homogeneous and heterogeneous anisotropic head model forward problem results. The color (or – in the printed version of this article – gray level) of each point indicates the corresponding NRDM of a dipolar source located at that point.

model are an average of many subjects, thus it is spatially smoothed compared to an individual conductivity tensor map, so the effect of the heterogeneity and anisotropy in a particular subject might be larger than in the presented results. We consider this error to be significative, but note that this is only an example. It is clear that the localization error depends on the configuration of the depth electrodes, the electric conductivity map, and the adopted source model.

The source model is clearly another point of interest (Lachaux et al., 2003). We adopted a dipolar model because the forward problem results are easy to interpret and extrapolate to distributed source, e.g. the sensitivity to a distributed source can be obtained by averaging the sensitivity maps of Fig. 2, weighted by the intensity of the distributed source at each point. While distributed sources can be approximated by a set of dipoles (Jerbi et al., 2004; von Ellenrieder et al., 2009), it should be done with care in the case of intracerebral electrodes. Given the sharp sensitivity profile of the electrodes, the approximation should be done with a set of dipoles placed very near to each other.

The results obtained in this work correspond to sEEG depth electrodes. While some of the results may apply also to ECoG electrodes, the nonconducting substrate holding the electrodes in this case is much larger, and could produce larger perturbations in the electric potential distribution (Zhang et al., 2006). The nonconducting contacts approximation could be of interest in this case. Regarding the model of the brain, since the cortical electrodes are placed outside the gray matter, probably the anisotropy of the white matter has a limited effect, but the larger conductivity of the CSF may have an important role, as in scalp EEG (Wolters et al., 2006).

We would like to point out that according to the literature, the depth electrodes record activity of sources located very near to the contacts (Mitzdorf, 1987; Juergens et al., 1999; Logothetis, 2003; Zaveri et al., 2009). This is in agreement with our results showing a sharp decrease in sensitivity with the distance between source and contact. However, this may lead to an inexact idea that the activity of sources farther away can not be sensed with this kind of electrodes. Actually, this activity is also recorded, but with a lower amplitude. Then, if there is activity near the contact it may complicate the detection of the farther sources, but in some cases it is still possible (Wennberg and Lozano, 2003; Acar et al., 2008; Wennberg, 2010; Wendel et al., 2011), and the source estimation algorithms have the potential to take advantage of this.

We consider this study of the appropriate models as a necessary first step in the solution of the stereo-EEG inverse problem. We found that an ideal point-size electrode that does not disturb the electric potential distribution is an appropriate model for depth electrode's contacts. Regarding the model for the brain, it is clear that if the detailed electric conductivity map of the subject is available an heterogeneous anisotropic brain model will lead to better inverse problem results. If such a map is not available the inverse problem errors associated to the homogeneous isotropic brain model analyzed in this work will interact, in a non-linear fashion, with other error sources. It is quite possible that in such a situation the dominant factor would be the neural activity unrelated to the phenomena under study, taking place in the proximity of the electrode contacts. In such a situation, a detailed brain model may be unnecessary.

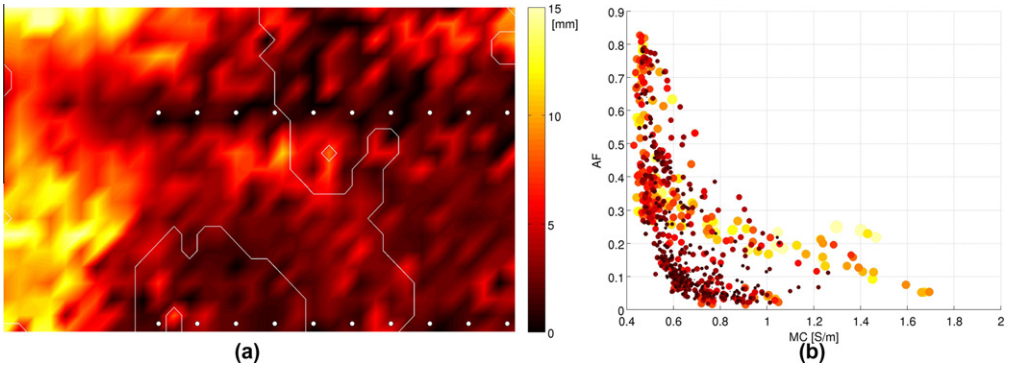

Fig. 9. Localization error for a single dipolar source due to homogeneous isotropic brain model approximation. (a) The color (or – in the printed version of this article – gray level) of each point indicates the localization error obtained for a source at that point. The white points correspond to contact positions, the lower ones are actually 15 mm over and under the plane of the figure. The white lines delimitate the gray matter. (b) Scatter plot of the localization error as a function of the mean conductivity (MC) and anisotropy factor (AF) of the point at which the source is located. Each point correspond to one of the sources in (a). The color (or – in the printed version of this article – gray level) and size of the points indicates the localization error.

Acknowledgements

The authors thank Dr. Jean Gotman of the Montreal Neurological Institute for his valuable insights and comments.

This work was funded by the Argentinian Ministerio de Ciencia y Tecnología Grant PICT 2007-00535 and Universidad Nacional de La Plata Grant 11-I127.

Appendix A

To obtain the integral formulation of the differential problem (1) we proceed as for scalp EEG forward problems (Geselowitz, 1967; de Munck, 1992). The only differences are that in this case we solve the exterior problem (by choosing appropriately the normal direction on the surfaces), and that for the conducting parts of the surface there is a mixed boundary condition. Starting from Green's Theorem

$$\int_\Omega (\varphi(\boldsymbol{y})\nabla^2\psi(\boldsymbol{y}) - \psi(\boldsymbol{y})\nabla^2\varphi(\boldsymbol{y}))d^3y = \int_S (\varphi(\boldsymbol{y})\nabla\psi(\boldsymbol{y}) - \psi(\boldsymbol{y})\nabla\varphi(\boldsymbol{y}))\cdot\boldsymbol{n}(\boldsymbol{y})ds(\boldsymbol{y}), \quad (10)$$

by choosing $\varphi(\boldsymbol{y}) = \sigma\phi(\boldsymbol{y})$ and $\psi(\boldsymbol{y}) = |\boldsymbol{y}-\boldsymbol{x}|^{-1}$, so that $\nabla^2\psi(\boldsymbol{y}) = 4\pi\delta(\boldsymbol{x}-\boldsymbol{y})$ (a Dirac delta), choosing the domain Ω as the exterior of the electrode and S as its boundary, we get

$$c(\boldsymbol{x})\phi(\boldsymbol{x}) = 4\pi\phi_0(\boldsymbol{x}) - \int_S \phi(\boldsymbol{y})\nabla\frac{1}{|\boldsymbol{x}-\boldsymbol{y}|}\cdot\boldsymbol{n}(\boldsymbol{y})ds(\boldsymbol{y}) + \int_S \frac{1}{|\boldsymbol{x}-\boldsymbol{y}|}\nabla\phi(\boldsymbol{y})\cdot\boldsymbol{n}(\boldsymbol{y})ds(\boldsymbol{y}), \quad (11)$$

where $c(\boldsymbol{x})/(4\pi)$ is the proportion of the surface area of a sphere of infinitesimal radius that lays inside the domain Ω (de Munck, 1992), $\phi_0(\boldsymbol{x}) = (-1/4\pi\sigma)\int_\Omega |\boldsymbol{x}-\boldsymbol{y}|^{-1}\nabla\cdot\boldsymbol{J}_0(\boldsymbol{y})d^3y$ is the electric potential generated by the source in an infinite medium. Since $\nabla\phi(\boldsymbol{y})\cdot\boldsymbol{n}(\boldsymbol{y}) = 0$ on the non-conducting surfaces, and $z\sigma\nabla\phi(\boldsymbol{y})\cdot\boldsymbol{n}(\boldsymbol{y}) = \Phi_k - \phi(\boldsymbol{y})$ on the surface of the k-th conducting contact, replacing this in (11) we get the integral problem formulation (2).

To solve the integral Eq. (2) with the Boundary Elements Method, the surfaces are tessellated in a set of plane triangles, and a linear approximation of the electric potential is adopted on each triangle. In this way the electric potential on the surfaces is completely determined by the electric potential on the vertices or nodes of the surface tessellation, and the problem results in a linear system of equations. To compute the coefficients of the linear system it is necessary to compute several integrals.

$$\int_\triangle h(\boldsymbol{y})\nabla\frac{1}{|\boldsymbol{x}-\boldsymbol{y}|}\cdot\boldsymbol{n}(\boldsymbol{y})ds(\boldsymbol{y}), \quad (12)$$

$$\int_\triangle \frac{1}{|\boldsymbol{x}-\boldsymbol{y}|}ds(\boldsymbol{y}), \quad (13)$$

$$\int_\triangle \frac{h(\boldsymbol{y}}{|\boldsymbol{x}-\boldsymbol{y}|}ds(\boldsymbol{y}), \quad (14)$$

where the domain is any plane triangle of the surface tessellation, and $h(\boldsymbol{y})$ is a linear function equal to 1 at one of the vertices of the triangle and zero on the other two vertices. Analytic expressions for computing (12) and (13) can be found in the literature (de Munck, 1992; Ferguson et al., 1994). While analytic expressions for computing (14) can also be obtained, they are very involved and we considered convenient to approximate this integral with a Gaussian quadrature integration scheme. Each triangle is linearly transformed into an equilateral triangle centered at the origin and on the x-y plane, circumscribing a circle of radius 1. We use a seven points rule (Abramowitz and Stegun, 1970, p. 893), then $\int_\triangle f(x,y)dxdy \approx \sum_{i=1}^7 w_i f(x_i,y_i)$, with the seven evaluation points $(0,0);((\sqrt{15}+1)/7,0);(-(\sqrt{15}+1)/14,\pm\sqrt{3}(\sqrt{15}+1)/14);\ (-(\sqrt{15}-1)/7,0);((\sqrt{15}-1)/14,\pm\sqrt{3}(\sqrt{15}-1)/14)$ and the corresponding weights $w_i, 270/1200, (155-\sqrt{15})/1200, (155-\sqrt{15})/1200,\ (155-\sqrt{15})/1200,\ (155+\sqrt{15})/1200, (155+\sqrt{15})/1200, (155+\sqrt{15})/1200$.

References

Abramowitz M, Stegun IA. Handbook of mathematical functions. New York: Dover; 1970.
Acar ZA, Makeig S, Worrell G. Head modeling and cortical source localization in epilepsy. In: Proceedings of the 30th annual international conference of the IEEE Engineering in Medicine and Biology Society; 2008. p. 3763–6.
Bechtereva N, Abdullaev Y. Depth electrodes in clinical neurophysiology: neuronal activity and human cognitive function. Int J Psychophysiol 2000;37:11–29.
Benbadis SR, Wyllie E, Bingaman W. Intracranial EEG and localization studies. In: Wyllie E, Cascino GD, Gidal BE, Goodkin HP, editors. The treatment of epilepsy: principles and practice. Philadelphia: Lippincott; 2005. p. 1059–67.
Blount JP, Cormier J, Kim H, Kankirawatana P, Riley KO, Knowlton RC. Advances in intracranial monitoring. Neurosurg Focus 2008;25:E18.
Brebbia CA, Dominguez J. Boundary elements. An introductory course. 2nd ed. Computational Mechanics Publications. McGraw-Hill; 1992.
Cabral B, Leedom L. Imaging vector fields using line integral convolution. In: Proceedings of SIGGRAPH 1993 conference; 1993. p. 263–72.
Chang N, Gulrajani R, Gotman J. Dipole localization using simulated intracerebral EEG. Clin Neurophysiol 2005;116:2707–16.
Châtillon CE, Zelmann R, Bortel A, Avoli M, Gotman J. Contact size does not affect high frequency oscillation detection in intracerebral EEG recordings in a rat epilepsy model. Clin Neurophysiol 2011;122:1701–5.
Cheng KS, Isaacson D, Newell J, Gisser D. Electrode models for electric current computed tomography. IEEE Trans Biomed Eng 1989;36:918–24.
Cho JH, Hong SB, Jung YJ, Kang HC, Kim HD, Suh M, et al. Evaluation of algorithms for intracranial EEG (iEEG) source imaging of extended sources: feasibility of using iEEG source imaging for localizing epileptogenic zones in secondary generalized epilepsy. Brain Topogr 2011;24:91–104.
Dannhauer M, Lanfer B, Wolters C, Knosche T. Modeling of the human skull in EEG source analysis. Hum Brain Mapp 2011;32:1383–99.
Dümpelmann M, Fell J, Wellmer J, Urbach H, Elger CE. 3D source localization derived from subdural strip and grid electrodes: a simulation study. Clin Neurophysiol 2009;120:1061–9.
von Ellenrieder N, Valdés-Hernández P, Muravchik C. On the EEG/MEG forward problem solution for distributed cortical sources. Med Biol Eng Comput 2009;47:1083–91.
Engel AK, Moll CKE, Fried I, Ojemann GA. Invasive recordings from the human brain: clinical insights and beyond. Nat Rev Neurosci 2005;6:35–47.
Fang Q, Boas D. Tetrahedral mesh generation from volumetric binary and gray-scale images. In: Proceedings of the IEEE international symposium on biomedical imaging; 2009. p. 1142–5.
Ferguson AS, Zhang X, Stroink G. A complete linear discretization for calculating the magnetic field using the boundary element method. IEEE Trans Biomed Eng 1994;41:455–60.
Geselowitz DB. On bioelectric potentials in an inhomogenous volume conductor. Biophys J 1967;7:1–11.
Halgren E, Baudena P, Heit G, Clarke M, Marinkovic K. Spatio-temporal stages in face and word processing. 1. Depth recorded potentials in the human occipital and parietal lobes. J Physiol Paris 1994;88:1–50.
Jenkinson M, Pechaud M, Smith S. BET2: MR–based estimation of brain, skull and scalp surfaces. In: Proceedings of the eleventh annual meeting of the Organization for Human Brain Mapping; 2005.
Jerbi K, Baillet S, Mosher JC, Nolte G, Garnero L, Leahy RM. Localization of realistic cortical activity in MEG using current multipoles. Neuroimage 2004;22:779–93.
Jerbi K, Ossandón T, Hamamé CM, Senova S, Dalal SS, Jung J, et al. Task-related gamma-band dynamics from an intracerebral perspective: Review and implications for surface EEG and MEG. Hum Brain Mapp 2009;30:1758–71.
Juergens E, Guettler A, Eckhorn R. Visual stimulation elicits locked and induced gamma oscillations in monkey intracortical- and EEG-potentials, but not in human EEG. Exp Brain Res 1999;129:247–59.
Kay SM. Fundamentals of statistical signal processing: estimation theory. Signal processing series. Prentice-Hall; 1993.
Kobayashi K, Yoshinaga H, Ohtsuka Y, Gotman J. Dipole modeling of epileptic spikes can be accurate or misleading. Epilepsia 2005;46:397–408.
Lachaux J, Rudrauf D, Kahane P. Intracranial EEG and human brain mapping. J Physiol Paris 2003;97:613–28.
Litvak V, Eusebio A, Jha A, Oostenveld R, Barnes GR, Penny WD, et al. Optimized beamforming for simultaneous MEG and intracranial local field potential recordings in deep brain stimulation patients. Neuroimage 2010;50:1578–88.
Logothetis NK. The underpinnings of the bold functional magnetic resonance imaging signal. J Neurosci 2003;23:3963–71.
Mazziotta J, Toga A, Evans A, Fox P, Lancaster J, Zilles K, et al. A probabilistic atlas and reference system for the human brain: International consortium for brain mapping (ICBM). Philos Trans R Soc Lond B Biol Sci 2001;356:1293–322.
Meijs JWH, Weier OW, Peters MJ, van Oosterom A. On the numerical accuracy of the boundary element method. IEEE Trans Biomed Eng 1989;36:1038–49.

Merlet I, Gotman J. Reliability of dipole models of epileptic spikes. Clin Neurophysiol 1999;110:1013–28.
Mitzdorf U. Properties of the evoked-potential generators – current source-density analysis of visually eoked-potentials in the cat cortex. Int J Neurosci 1987;33:33–59.
Mori S, Oishi K, Jiang H, Jiang L, Li X, Akhter K, et al. Stereotaxic white matter atlas based on diffusion tensor imaging in an ICBM template. Neuroimage 2008;40:570–82.
de Munck JC. A linear discretization of the volume conductor boundary integral equation using analytically integrated elements. IEEE Trans Biomed Eng 1992;39:986–90.
de Munck JC, van Dijk BW, Spekreijse H. Mathematical dipoles are adequate to describe realistic generators of human brain activity. IEEE Trans Biomed Eng 1988;35:960–6.
Ollikainen J, Vauhkonen M, Karjalainen PA, Kaipio JP. Effects of electrode properties on EEG measurements and a related inverse problem. Med Eng Phys 2000;22:535–45.
Paulson K, Breckon W, Pidcock M. Electrode modelling in electrical impedance tomography. SIAM J Appl Math 1992;52:1012–22.
Shenoy P, Miller K, Ojemann J, Rao R. Generalized features for electrocorticographic BCIs. IEEE Trans Biomed Eng 2008;55:273–80.
Somersalo E, Cheney M, Isaacson D. Existence and uniqueness for electrode models for electric current computed tomography. SIAM J Appl Math 1992;52:1023–40.
Tuch D, Wedeen V, Dale A, George J, Belliveau J. Conductivity tensor mapping of the human brain using diffusion tensor MRI. Proc Natl Acad Sci USA 2001;98:11697–701.
Wendel K, GN. N, Hannula M, Hyttinen J, Malmivuo J. The influence of electrode size on EEG lead field sensitivity distributions. In: International Journal of Bioelectromagnetism. Special Issue on Recent Trends in Bioelectromagnetism. 6th International Conference on Bioelectromagnetism, vol. 9. Aizu-Wakamatsu City, Fukushima, Japan; 2007. p. 116–7.
Wendel K, Suominen K, Kauppinen P, Sonkajarvi E, Tanskanen J, Kamata K, et al. Recording cortical EEG subcortically – improved EEG monitoring from depth-stimulation electrodes. In: Noninvasive Functional Source Imaging of the Brain and Heart 2011, 8th International Conference on Bioelectromagnetism (NFSI ICBEM); 2011. p. 126–30.
Wennberg R. On electrical potentials observed at a distance from intracranial electrode contacts. Clin Neurophysiol 2010;121:259–62.
Wennberg RA, Lozano AM. Intracranial volume conduction of cortical spikes and sleep potentials recorded with deep brain stimulating electrodes. Clin Neurophysiol 2003;114:1403–18.
Wolters CH, Anwander A, Tricoche X, Weinstein D, Koch MA, MacLeod RS. Influence of tissue conductivity anisotropy on EEG/MEG field and return current computation in a realistic head model: a simulation and visualization study using high-resolution finite element modeling. Neuroimage 2006;30:813–26.
Zaveri HP, Duckrow RB, Spencer SS. Concerning the observation of an electrical potential at a distance from an intracranial electrode contact. Clin Neurophysiol 2009;120:1873–5.
Zhang Y, Ding L, Van Drongelen W, Hecox K, Frim DM, He B. A cortical potential imaging study from simultaneous extra- and intracranial electrical recordings by means of the finite element method. Neuroimage 2006;31:1513–24.
Zhang Y, Van Drongelen W, Kohrman M, He B. Three-dimensional brain current source reconstruction from intra-cranial ECoG recordings. Neuroimage 2008;42:683–95.